Developmental Cell, Vol. 7, 559–569, October, 2004, Copyright ©2004 by Cell Press

ESCRT-II, an Endosome-Associated Complex Required for Protein Sorting: Crystal Structure and Interactions with ESCRT-III and Membranes

Hsiangling Teo, Olga Perisic, Beatriz González, and Roger L. Williams*
MRC Laboratory of Molecular Biology
Hills Road
Cambridge CB2 2QH
United Kingdom

Summary

ESCRT-I, -II, and -III protein complexes are sequentially recruited to endosomal membranes, where they orchestrate protein sorting and MVB biogenesis. In addition, they play a critical role in retrovirus budding. Structural understanding of ESCRT interaction networks is largely lacking. The 3.6 Å structure of the yeast ESCRT-II core presented here reveals a trilobal complex containing two copies of Vps25, one copy of Vps22, and the C-terminal region of Vps36. Unexpectedly, the entire ESCRT-II core consists of eight repeats of a common building block, a "winged helix" domain. Two PPXY-motifs from Vps25 are involved in contacts with Vps22 and Vps36, and their mutation leads to ESCRT-II disruption. We show that purified ESCRT-II binds directly to the Vps20 component of ESCRT-III. Surprisingly, this binding does not require the protruding N-terminal coiled-coil of Vps22. Vps25 is the chief subunit responsible for Vps20 recruitment. This interaction dramatically increases binding of both components to lipid vesicles in vitro.

Introduction

Downregulation and subsequent degradation of membrane receptors involves two ubiquitin-dependent membrane budding steps (Bonifacino and Traub, 2003; Hicke and Dunn, 2003; Katzmann et al., 2002; Peschard and Park, 2003; Raiborg et al., 2003). In the first step, the plasma membrane containing clustered ubiquitinated receptors buds inward to form vesicles that are delivered to endosomes. In the second step, the endosomal membrane buds away from the cytosol to form vesicles within the endosome. As the endosome accumulates internal vesicles, it takes on a morphology known as a multivesicular body (MVB). The limiting membrane of the MVB eventually fuses with the lysosomal membrane to expose the internal vesicles to the hydrolytic contents of the lysosome (Gruenberg and Stenmark, 2004; Piper and Luzio, 2001). In addition to this traffic from the plasma membrane, biosynthetic cargo is transported from the late Golgi via MVBs to the vacuolar lumen.

Formation of inward-budded vesicles from the endosomal membrane is controlled by cytosolic factors that are not related to the factors that control endocytosis. Genetic screens in yeast identified 18 class E *vps* mutants that have defects in sorting proteins into MVBs. Ten of these proteins are part of three multiprotein complexes (reviewed in Conibear, 2002; Katzmann et al., 2002; Morita and Sundquist, 2004). These are the 350 kDa ESCRT-I complex (consisting of Vps23, Vps28, and Vps37) (Katzmann et al., 2001), the 155 kDa ESCRT-II complex (Vps22, Vps25, and Vps36) (Babst et al., 2002b), and the ESCRT-III complex (Vps2, Vps24, Vps20, and Vps32) (Babst et al., 2002a). Each of these complexes has human orthologs that are required for lysosomal traffic. The human ESCRT-I complex consists of Tsg101 (Vps23 homolog) (Babst et al., 2000; Garrus et al., 2001; Li and Cohen, 1996), hVps28 (Bishop and Woodman, 2001), and the recently identified Vps37 homologs hVps37A and hVps37B (Bache et al., 2004; Stuchell et al., 2004), while the human ESCRT-II subunits correspond to EAP20 (Vps25), EAP30 (Vps22), and EAP45 (Vps36) (Kamura et al., 2001; Schmidt et al., 1999). The ESCRT-III components Vps2, Vps24, Vps32/Snf7, and Vps20 are homologous with the human proteins CHMP2A, CHMP3, CHMP4B, and CHMP6, respectively (Martin-Serrano et al., 2003; von Schwedler et al., 2003).

Many of the cargo proteins destined for delivery to vacuoles or lysosomes are monoubiquitinated (Katzmann et al., 2001; Reggiori and Pelham, 2001; Urbanowski and Piper, 2001). Several ubiquitin-recognizing modules are present in the ESCRT complexes, including the UEV domain of Vps23 (Katzmann et al., 2001; Pornillos et al., 2002; Sundquist et al., 2004; Teo et al., 2004) and the NZF-finger domain of Vps36 (Alam et al., 2004). Deletion of Vps23 prevents formation of MVBs; however, this defect can be partially overcome by overexpression of ESCRT-II, suggesting that the ESCRT-II functions downstream of ESCRT-I (Babst et al., 2002b). ESCRT-II forms a stable, soluble complex of defined stoichiometry. In contrast, the ESCRT-III subunits are cytosolic and monomeric until they are recruited to membranes, a process that is dependent on ESCRT-II (Babst et al., 2002a).

Interactions within the ESCRT complexes have been extensively investigated by yeast two-hybrid analysis (Bowers et al., 2004; Martin-Serrano et al., 2003; von Schwedler et al., 2003). Within the ESCRT-II complex, all possible pairs of interactions among Vps22, Vps25, and Vps36 were reported. In addition, these studies also show interaction between ESCRT-II and ESCRT-III. Although the methodology does not unequivocally establish direct interactions, each of these studies showed an interaction between the ESCRT-III Vps20 subunit (or its human ortholog) and each of the components of the ESCRT-II complex. The ESCRT-III subunits share several features including an N-terminal half rich in basic residues, an acidic C-terminal half, and one or more regions predicted to have a coiled-coil architecture (Babst et al., 2002a). Although the ESCRT-III subunits are monomeric in the cytosol, in the context of a ΔVps4 mutant that is defective in disassembly of the ESCRT complexes, the ESCRT-III subunits colocalize on endosomal membranes and can be coimmunoprecipitated. It has been proposed that initiation of the recruitment

*Correspondence: rlw@mrc-lmb.cam.ac.uk

Table 1. Data Collection, Structure Determination, and Refinement Statistics

Data Collection and MAD Phasing Statistics						
	Se-Met SAD[a]	Se-Met MAD[b]				
Data set	Peak	Peak	Inflection	Remote	Native[c]	Sulfur[d]
Resolution	3.7	4.0	4.0	4.0	3.6	4.2
Completeness (last shell)	99.9 (99.9)	100 (100)	99.6 (99.6)	99.5 (99.5)	99.2 (95.3)	100 (100)
R_{merge}[e] (last shell)	0.071 (0.53)	0.12 (0.46)	0.11 (0.46)	0.12 (0.59)	0.068 (0.41)	0.11 (0.41)
Multiplicity (last shell)	14.1 (14.1)	14.3 (14.2)	11.6 (11.6)	7.2 (7.2)	6.9 (3.9)	24.9 (24.0)
$<I/\sigma>$ (last shell)	7.3 (1.4)	4.8(1.6)	4.9 (1.2)	4.5 (1.3)	4.4 (1.7)	3.9 (1.3)
Phasing Statistics						
Phasing power (iso)[f]	N/A	0.47	N/A	0.96		
Phasing power (anom)[f]	2.5	1.7	0.95	0.99		
Se sites found	19	19				
FOM after SHARP	0.41	0.30				
FOM after SOLOMON	0.70	0.66				
FOM after DM	0.83	0.78				
Refinement Statistics						
Resolution (number of reflections)	3.6 (23806)					
Protein atoms	6135					
R_{cryst}[g]	0.30					
R_{free}[g] (% data used)	0.34 (4.9)					
Rmsd from ideality[h]						
Bonds/angles/dihedrals	0.017/1.6/8.3					
Overall B (Wilson B factor)	65 (110)					

[a] Data set was collected at ESRF beamline BM14 at wavelength 0.97093 Å.
[b] Data sets were collected at ESRF beamline BM14 at wavelengths 0.97093 Å, 0.97925 Å, and 0.93927 Å for the peak, inflection, and remote data sets.
[c] Data set was collected at ESRF beamline ID23 at wavelength 1.055 Å.
[d] Data set was collected at Daresbury SRS beamline 10.1 at wavelength 2.07 Å.
[e] $R_{merge} = \Sigma_{hkl}\Sigma_i|I_i(hkl) - <I(hkl)>|/\Sigma_{hkl}\Sigma_i\ I_i(hkl)$.
[f] The phasing power is defined as the ratio of the rms value of the heavy atom structure factor amplitudes to the rms value of the lack-of-closure error.
[g] R_{cryst} and $R_{free} = \Sigma|F_{obs} - F_{calc}|/\Sigma\ F_{obs}$; R_{free} calculated with the percentage of the data shown in parentheses.
[h] Rms deviations for bond angles and lengths in regard to Engh and Huber parameters.

of the ESCRT-III complex is brought about by the myristoylated Vps20 subunit binding to ESCRT-II (Babst et al., 2002a). The presence of two predicted coiled-coil regions in Vps22 led to the speculation that binding of Vps20 to ESCRT-II might be mediated by coiled-coil interactions between Vps20 and Vps22 (Babst et al., 2002b).

To gain insight into the proposed role of ESCRT-II as a nucleus for the formation of the ESCRT-II/ESCRT-III network on endosomal membranes, we have determined the three-dimensional structure of yeast ESCRT-II, characterized the interactions that ESCRT-II makes with the Vps20 subunit of ESCRT-III, and shown that the Vps25 subunit of ESCRT-II forms a direct complex with Vps20, which greatly facilitates recruitment of both ESCRT-II and Vps20 to liposomes in vitro.

Results and Discussion

The three subunits of the yeast ESCRT-II complex were coexpressed in *E. coli*, and the purified complex crystallized in space group $P4_322$ with cell dimensions a = 150 Å and c = 186 Å. The 3.6 Å structure was solved by the multiple anomalous dispersion method with a selenomethione-substituted crystal. Furthermore, the register of the sequence in the electron density was verified using an additional data set collected to optimize the signal from the sulfurs of the Met and Cys residues (Supplemental Figure S1 at http://www.developmentalcell.com/cgi/content/full/7/4/559/DC1/). The structure of the complex shows that ESCRT-II contains two copies of Vps25 and one copy each of Vps22 and Vps36. No density is visible for residues 1–395 of Vps36 and residues 1–21 of Vps22. SDS-PAGE analysis of crystals showed that Vps36 had been partially proteolyzed, and the truncated form was preferentially incorporated into crystals. The complex formed from coexpressing an N-terminal truncation of Vps36 (residues 1–370 deleted) together with Vps22 and Vps25 resulted in identical crystals and no change in diffraction resolution. Although we obtained crystals with protein preparations having an intact Vps36, they diffracted only to very low resolution (~12 Å). Despite extensive efforts to improve the diffraction limit of the crystals, the highest resolution obtained was 3.4 Å and temperature factors for the complex are correspondingly large. Because of the relatively weak data at the resolution limit, the refinement was carried out to 3.6 Å resolution and the data collection statistics for this resolution are shown in Table 1. The structure of the ESCRT-II core complex shows that the N terminus of the truncated Vps36 construct is involved in a crystal

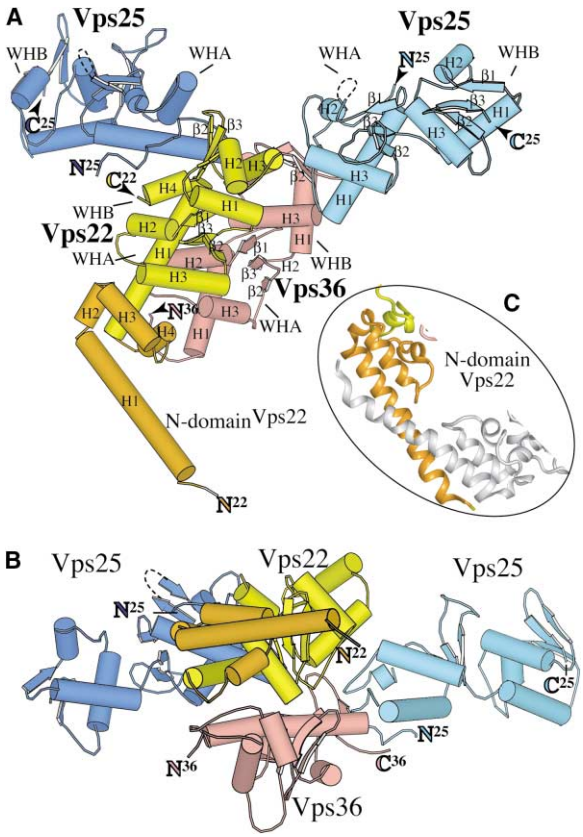

Figure 1. The ESCRT-II Complex Has a Trilobal Overall Structure

(A) Ribbon diagram of ESCRT-II, containing two Vps25 subunits (each making one lobe), and one copy of Vps22 and Vps36 subunit (tightly packed together into a third lobe). Only the C-terminal portion of Vps36 is ordered in the crystals. The protruding N-terminal helical domain of Vps22 subunit is colored orange, while its two winged helix domains are yellow; the Vps36 subunit is pink and the two Vps25 subunits are colored cyan and blue. The two winged helix (WH) domains in each subunit are labeled as WHA and WHB. The elements of secondary structure and the N and C termini are also indicated.

(B) A view of the complex approximately 90° from the view in (A), showing a rather flat "profile" of the complex.

(C) The crystallographic coiled-coil interaction of the Vps22 N-terminal helix. The asymmetric unit of the crystal contains one complex of ESCRT-II, but as a consequence of a crystal contact, the N-terminal helices of Vps22 molecules from two adjacent complexes pack together, forming an antiparallel coiled-coil (one molecule is colored orange, the other white). ESCRT-II is a monomer in solution, but potentially, the Vps22 N-terminal helix could form a coiled-coil dimer, either with another ESCRT-II complex or some other (currently unknown) binding partner.

contact, explaining why these crystals were not able to accommodate the full-length Vps36 despite having very high solvent content (72%) and large, continuous solvent voids.

The Overall Shape of ESCRT-II

The overall trilobal shape of the complex resembles the character τ, with the upper branches of the letter corresponding to two molecules of Vps25 and the stem representing the tightly packed Vps22 and Vps36 subunits (Figure 1). The first helix of the N-terminal 5-helix domain of Vps22 protrudes from the complex to form a prominent intermolecular interaction in the crystal. The dimensions of the complex are approximately 120 Å between the tips of the two Vps25 domains and 50 Å in thickness between the outer surfaces of the paired Vps22 and Vps36 subunits. Two structurally similar domains arranged head-to-tail give each of the subunits an oblong shape. The two Vps25 subunits are aligned approximately colinear with each other and related by a rotation angle of about 156°. The two Vps25 subunits make no direct contacts with each other. However, the N-terminal domain of one Vps25 subunit (molecule B) contacts the C-terminal domain of Vps22, and the other Vps25 subunit (molecule C) contacts Vps36, burying 1637 Å^2 and 1531 Å^2 surface area, respectively. In addition, Vps36 makes much less extensive contacts (444 Å^2) with the Vps25 molecule B. The interface of Vps22 with the Vps25 molecule C is minimal (155 Å^2).

The Vps22 and Vps36 subunits pair side-by-side along the long axis of their ellipsoids and bury 2669 Å^2 of surface area between them, suggesting a very tight interface. The extensive Vps22/Vps36 interface is consistent with the observation that neither Vps36 nor Vps22 can be expressed alone in *E. coli* (data not shown). Furthermore, no soluble complex was obtained when Vps22 and Vps36 were coexpressed in *E. coli* in the absence of Vps25. Although Vps25 forms stable interactions in the ESCRT-II complex, this subunit can be readily expressed, purified, and crystallized on its own.

The ESCRT-II Core Is Built from Eight Winged Helix Domains

Surprisingly, the structure shows that Vps22, Vps25, and Vps36 each contain two repeats of a domain with an H1/β1/H2/H3/β2/β3 topology that has been referred to as a "winged helix" (WH) domain, which is present in a variety of proteins—most notably transcription factors (Figure 2; Gajiwala and Burley, 2000). The three helices of each of the WH domains assemble beneath a small β sheet formed by the three antiparallel β strands. Within each subunit, the N-terminal WH domain (WHA) packs against the C-terminal WH domain (WHB) in a head-to-tail manner, with the exposed surface on the WHA β sheet interacting with ends of helices H1 and H3 of the WHB. All of the WH domains in the ESCRT-II complex superimpose on each other with an rms deviation less than 2 Å, although the three ESCRT-II subunits have no recognizable sequence similarity (Figure 3). These domains form the interactions that give rise to the ESCRT-II complex, as well as the interactions with the ESCRT-III subcomplexes, which are essential for MVB formation (see below).

In addition to the winged helix core, the structure of ESCRT-II has a prominent extension at the bottom of the Vps22/Vps36 stem, which protrudes away from the body of the complex. This extension represents part of the N-terminal 5-helix domain of Vps22 (residues 22–90). The first helix of this domain is a distinctly amphipathic helix that forms coiled-coil interactions with a 2-fold related copy of this helix from another complex in the crystal (Figure 1C). Although this 2-fold intermolecular interaction between Vps22 subunits is extensive in the

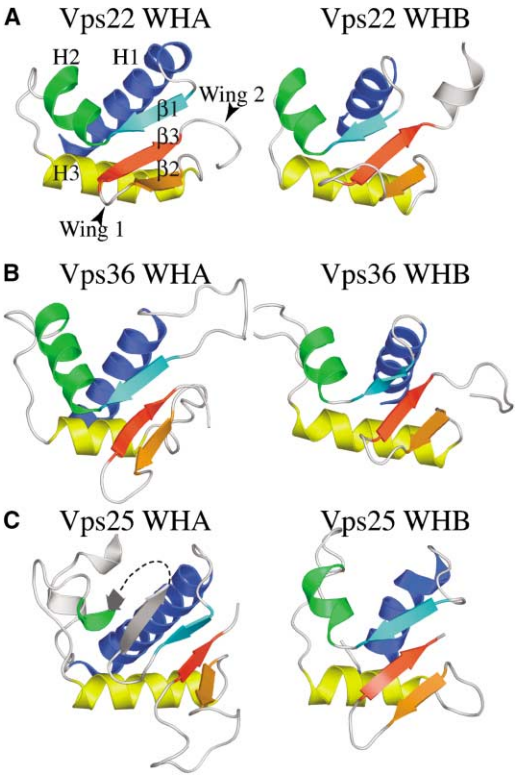

Figure 2. Each of the Three ESCRT-II Subunits Has Two Winged Helix Domains

WH domains have a small, three-stranded β sheet mounted on a helical base. Wing 1 and Wing 2 are segments preceding and following the last strand (β3). Ribbon diagrams are shown for the winged helix domains from (A) Vps22, (B) Vps36, and (C) Vps25 (molecule B). The secondary structure elements are colored in rainbow colors from blue (N terminus) to red (C terminus).

crystal (1681 Å^2 surface area buried in the interface), the ESCRT-II complex is a monomer in solution (Babst et al., 2002b). The last helix of this N-terminal domain extends into the first helix of the Vps22 WHA domain.

An Exposed Hydrophobic Surface Is a Common Protein-Protein Recognition Element in WH Domains

The canonical winged helix architecture includes two "wings," the β2/β3 loop referred to as Wing 1 and the long loop following β3 referred to as Wing 2 (Gajiwala and Burley, 2000). The ESCRT-II WH domains either lack or have very short Wing 2 extension (Figure 2). Like other winged helix domains, all of the secondary structure elements in the ESCRT-II winged helices have hydrophobic residues that interdigitate to form a hydrophobic core of the domain. Among the DNA binding WH domains, it is common that helix H3 fits into the minor groove to act as a recognition element. Furthermore, protein-protein interactions involving winged helix transcription factors use exposed hydrophobic patches (Clark et al., 1993; Finnin et al., 1997; Gajiwala and Burley, 2000). For example, the activation domain of the bacteriophage T4 transcription factor has a winged helix fold, and mutagenesis studies suggest that an exposed hydrophobic patch on the surface of the WH β sheet may be involved in protein-protein interactions that facilitate transcriptional activation. The analogous H3 and β sheet surfaces of the Vps22 and Vps36 WHB domains expose a series of hydrophobic residues that interact with Vps25. In addition, Vps25 has prominent exposed hydrophobic patches that could bind other proteins such as Vps20 (see below).

Interactions between the Vps22 and Vps36 Subunits

The yeast Vps22/Vps36 interaction surface is largely hydrophobic (Figure 4A), with several interspersed salt links. There are four salt links between the Vps22 WHA and Vps36 WHA domains; the residues forming these salt links are not conserved among Vps22 and Vps36 subunits from other species (Figure 4A). The contacts between the Vps22 and Vps36 N-terminal WH domains are more extensive than between the C-terminal WH domains. These WHA contacts involve helix H1 and the H3/β2 loop of Vps22. On the Vps36 side, the interactions involve helices H2 and H3 and the loops preceding them and connecting them. The Vps22/36 contacts in the WHB domains are more restricted and involve H3 of Vps22 and the β2/β3 loop (Wing 1) of Vps36.

Interactions of the Vps25 Subunits with Vps22 and Vps36

Whereas the Vps22/Vps36 subunits interact side-by-side using elements from both WH domains of each of the two subunits, the Vps22/Vps25 and Vps36/Vps25 interactions are a head-to-tail arrangement with the WHB of Vps22 or Vps36 contacting the WHA domain from one of the Vps25 subunits (Figure 1). These head-to-tail interactions involve almost exclusively the β2 and β3 strands, the β2/β3 loop (Wing 1), and the loop following β3 (Wing 2) of the Vps22 and Vps36 WHB domains, contrasting sharply with the side-to-side Vps22/36 interactions involving primarily helical elements and connecting loops. The binding site on the Vps25 subunit involves an N-terminal segment encompassing the PPXY motifs, H1 residues, and the strictly conserved Arg83 from the WHA domain.

Two Tandem PPXY Motifs in Vps25 Are Central to Intersubunit Interactions

Residues 1–19 of Vps25 include two helical turns that encompass two conserved PPXY motifs, 5-PPVY-8 and 11-PPLY-14. PPXY motifs are often ligands for WW domains, and the Rsp5/Nedd4 ubiquitin ligase, an enzyme that plays an essential role in endosomal protein sorting, is recruited by these motifs (Dunn and Hicke, 2001; Hettema et al., 2004; Katzmann et al., 2004). However, in ESCRT-II these motifs are involved in intermolecular contacts within the complex. Both PPXY motifs from one Vps25 interact with Vps22. Very similar interactions are made between the second copy of Vps25 and Vps36 (Figures 4B and 4C). The Vps25 interface with Vps22 and Vps36 is centered on the strictly conserved Phe10^{Vps25}, which sticks like a ball-in-socket into a hydrophobic pocket on Vps22 (lined with Trp212, Trp224, Pro226, Trp228, and Ile229) or Vps36 (lined with Leu545, Leu546, Ile547, Tyr557, and Tyr561). Pro6 from the first 5-PPXY-8 motif as well as both proline residues from the second

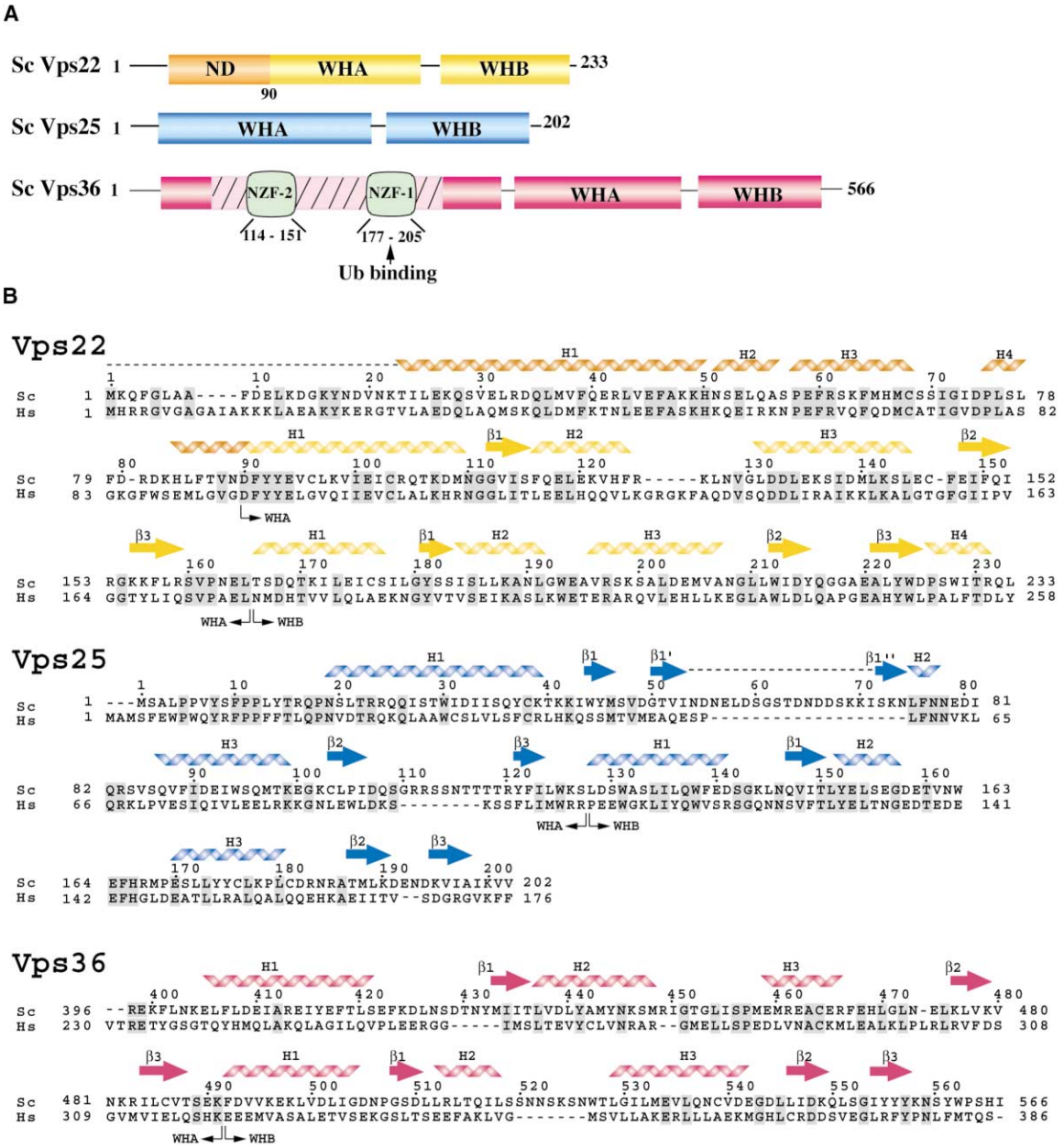

Figure 3. A Schematic Illustration of the Domain Organization and Sequence Alignments of the ESCRT-II Subunits

(A) WHA denotes winged helix A and WHB denotes winged helix B. ND denotes N-terminal helical domain in Vps22, and NZF stands for Npl4 zinc fingers in Vps36. Sc denotes *Saccharomyces cerevisiae*. Only the NZF-1 domain binds ubiquitin (Alam et al., 2004). The hatched region in Vps36 represents an insertion in the yeast sequence relative to human. Consequently, NZF domains are absent in human Vps36.

(B) Sequence alignments of yeast (Sc) and human (Hs) ESCRT-II sequences with secondary structure elements indicated above the yeast subunits. Dashed lines indicate disordered regions.

PPXY motif (11-PP-12) make hydrophobic interactions with Vps22. Equivalent interactions are formed between Vps36 and the second copy of Vps25. Although the tyrosines of the PPXY motifs make no direct contact with either the Vps22 or Vps36 subunits, they buttress the Pro-Pro motifs against the 76–85 region of the Vps25 WHA. A Vps25 double mutant, Y8A/Y14A, when coexpressed with Vps22 and Vps36, yielded only free Vps25 and no intact complex (Vps22 and Vps36 coexpression in *E. coli* in the absence of Vps25 yields no soluble protein), indicating the central importance of these interactions for ESCRT-II formation.

Conserved Salt Links Stabilize the Interactions of Vps25 with Vps22 and Vps36

In addition to nonpolar interactions that appear to dominate the Vps25/Vps22 interface, there is a salt link between Arg83 of Vps25 and Asp214 in the WHB domain of Vps22 (Figure 4). Both of these residues are conserved in Vps22 and Vps25 subunits from other species. The

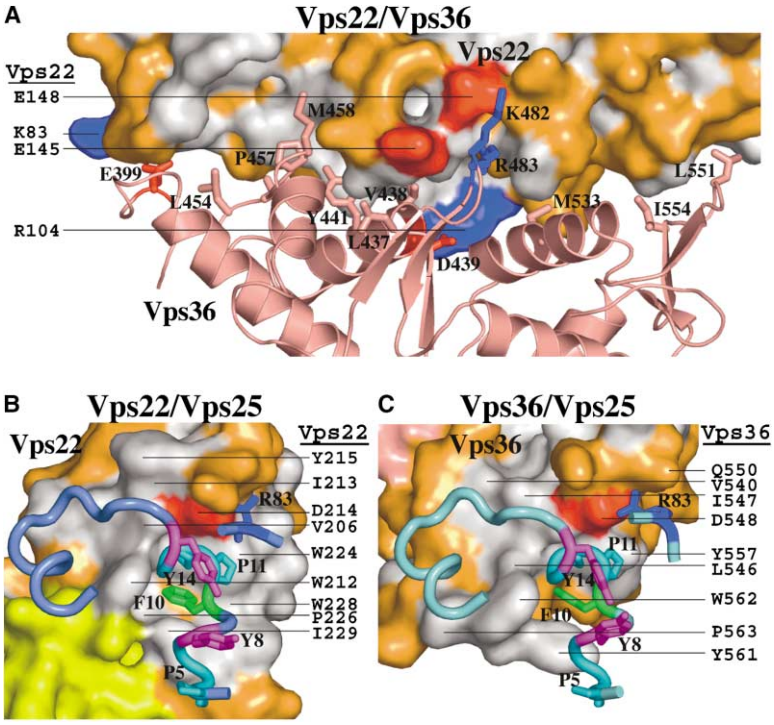

Figure 4. Hydrophobic Interactions Intersperse with a Few Salt Links to Form the Intersubunit Contacts in ESCRT-II

In solid surface representation, hydrophobic residues are colored white, residues involved in intersubunit salt links are colored red (acidic) and blue (basic), and the rest of the residues are colored bronze.

(A) The interface between Vps22 (solid surface) and Vps36 (pink ribbon) involves both WH domains from both subunits. Vps36 residues making hydrophobic interactions are shown as pink sticks, and those forming salt links are blue or red sticks.

(B) The interface between the WHB domain of Vps22 (solid surface) with the WHA domain of Vps25 (blue worm) is predominantly hydrophobic and includes proline residues from the PPXY motifs in Vps25 (cyan). Phe10^{Vps25} (green) at the junction between the two PPXY motifs fits into a hydrophobic pocket on Vps22. Neither of the tyrosines (purple) from the PPXY motifs interacts with Vps22. Conserved residues forming a salt bridge between the two molecules (Asp214^{Vps22} and Arg83^{Vps25}) are highlighted. The locations of some of the interacting residues from Vps22 are also indicated.

(C) The interface between the WHB domain of Vps36 (solid surface) with the second copy of Vps25 (light blue worm) shows similar features as Vps22/25 interface, including the hydrophobic "ball-joint" formed by Phe10^{Vps25}, interactions with the PPXY motifs, and the salt bridge between the Asp548^{Vps36} and Arg83^{Vps25}.

second molecule of Vps25 in the ESCRT-II complex makes equivalent interactions with the WHB domain of Vps36, which is pseudo-symmetric with the WHB domain of Vps22. An analogous salt link is formed between Arg83 of Vps25 and Asp548 of Vps36. Similarly to Asp214 of Vps22, Asp548 of Vps36 is conserved in other species.

ESCRT-II Interacts Directly with Vps20 Subunit from ESCRT-III

Both genetic and biochemical data indicate that ESCRT-II interacts with Vps20 (Babst et al., 2002b; Bowers et al., 2004; Martin-Serrano et al., 2003; von Schwedler et al., 2003), and it was shown that this interaction plays an important role in the formation of ESCRT-III complex (Babst et al., 2002a). However, because all the current evidence is based on yeast two-hybrid interactions or pull-down assays using yeast extract, it is not clear whether the interaction is direct or indirect, via an unknown bridging molecule. We used purified ESCRT-II and Vps20 to examine whether they can interact directly in vitro. Using GST-tagged Vps20 and pull-down assays, we could demonstrate direct, specific interaction between full-length ESCRT-II and Vps20 that results in all three ESCRT-II subunits being retained by GST-Vps20 on glutathione beads (Figure 5A).

The Protruding N-Terminal Coiled-Coil Region of Vps22 Does Not Bind Vps20

The next question is which ESCRT-II subunit(s) is responsible for interaction with Vps20. It was previously proposed that the predicted coiled-coil regions of Vps22 could bind to coiled-coils of Vps20 (Babst et al., 2002b). In light of the ESCRT-II crystal structure, which shows that the N-terminal helix of Vps22 protrudes from the stem of the complex and makes coiled-coil interactions with and adjacent complex in the crystal, this was a very attractive proposal. To test this, we made an N-terminal truncation of Vps22 (residues 1–40 deleted) that removes most of the protruding helix H1 of the N-terminal domain and coexpressed and purified the ESCRT-II complex. This truncation had no noticeable affect on complex formation, as expected based on the lack of interactions of this helix with the rest of the complex. Surprisingly, the truncated complex bound as well as full-length ESCRT-II to GST-Vps20 (Figures 5A and 5B), showing that the N-terminal helix of Vps22 is not responsible for interaction with Vps20. In addition, the purified N-terminal fragment of Vps22 (residues 1–90, which we could purify in large amounts [50 mg/l *E. coli* culture]) did not show any binding to Vps20 (data not shown), confirming that the N-terminal helical domain of Vps22 is neither necessary nor sufficient for Vps20 interaction. Currently, we cannot exclude the possibility that this N-terminal helical domain of Vps22 could be involved in coiled-coil interactions with some other ESCRT-III subunit. However, comprehensive yeast two-hybrid analysis of human ESCRT-II/ESCRT-III interactions did not detect any interaction of ESCRT-II other than with Vps20 subunit of ESCRT-III, suggesting that Vps22-mediated coiled-coil interactions with ESCRT-III are not likely (Bowers et al., 2004; Martin-Serrano et al., 2003; von Schwedler et al., 2003).

In addition, we show that ESCRT-II complexes in which the N terminus of Vps36 is truncated (residues 1–370 deleted) do not affect binding to Vps20 (Figure 5B). This region of Vps36 is, however, necessary for

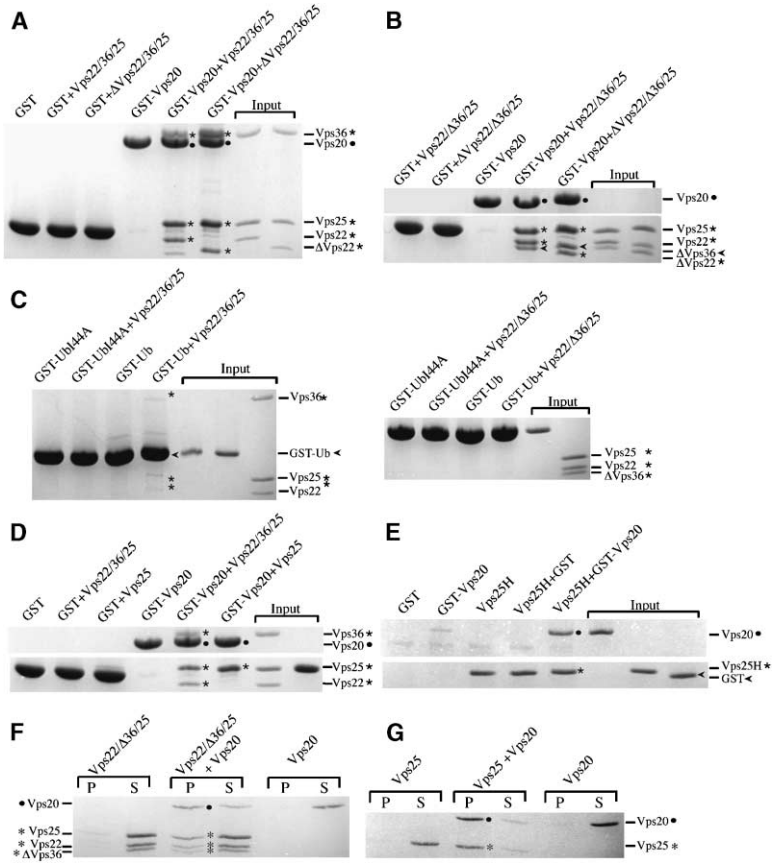

Figure 5. ESCRT-II Interacts Directly with the Vps20 Component of the ESCRT-III Complex via Vps25, which Greatly Increases Binding of Both Partners to Membranes

GST-Vps20 was incubated with either full-length ESCRT-II or with ESCRT-II complexes containing N-terminally truncated Vps36 (residues 1–370 deleted, ΔVps36) or Vps22 (residues 1–40 deleted, ΔVps22). The reactions were incubated with glutathione resin, and washed and the bound proteins were eluted with SDS sample buffer and analyzed by SDS-PAGE and Coomassie staining.

(A) Binding of ESCRT-II to Vps20 does not require the N-terminal 40 residues of Vps22.

(B) Binding of ESCRT-II to Vps20 does not require the N-terminal 370 residues of Vps36.

(C) Full-length ESCRT-II binds to GST-Ub, but not to a GST-Ubl44A (a mutant of the "I44"-patch on Ub shown to be important for endocytosis of ubiquitinated proteins [Sloper-Mould et al., 2001]). Right panel shows that ESCRT-II complex with truncated Vps36 (1–370 residues deleted) does not interact with GST-Ub.

(D) Isolated Vps25 alone interacts with GST-Vps20.

(E) Reciprocal assays using talon metal affinity beads and His-tagged Vps25 to pull down GST-tagged Vps20. Input lanes contain 0.16% of total protein added to assay.

(F and G) Purified ESCRT-II binds to lipid vesicles in vitro and greatly increases binding of Vps20 to membranes. Purified proteins, 5 μM each, either alone or mixed together, were incubated with brain liposomes and sedimented by ultracentrifugation.

(F) Lipid binding of either ESCRT-II alone (Vps22/Δ36/25, i.e., with N-terminal 1–370 residues of Vps36 deleted), of Vps20 alone, or of the two components together.

(G) Lipid binding of isolated Vps25 either alone or together with Vps20. When mixed together, both proteins bind to membranes much more efficiently than either protein alone. Pellets (P) were resuspended in the same volume as the supernatants (S), and equal volumes of the two fractions were analyzed by SDS-PAGE and Coomassie blue staining.

interaction of ESCRT-II with ubiquitin (Figure 5C), since its deletion greatly reduces the binding of purified truncated ESCRT-II to GST-ubiquitin using GST pull-down assays (Figure 5C). These results are consistent with recent findings that the NZF-1 domain from yeast Vps36 (residues 177–205) binds specifically to ubiquitin (Alam et al., 2004).

The Vps25 Subunit Interacts Directly with Vps20

We next tested whether Vps25 subunit could interact with Vps20. The structure shows that only the tips of the Vps25 subunits are involved in contacts with the other two ESCRT-II subunits, and most of the Vps25 surface is accessible for other interactions. Using purified Vps25 and Vps20, we show direct interaction between these two subunits (Figures 5D and 5E). Specific binding of the two proteins is demonstrated by pull-downs both on glutathione resin via GST-tagged Vps20 (Figure 5D) and on Ni-resin via His6-tagged Vps25 (Figure 5E). We could also demonstrate binding by band-shift analysis on native gels, as the electrophoretic mobility of the Vps20/Vps25 protein complex drastically differs from nonbound proteins (data not shown). The interaction between Vps20 and Vps25 is likely to be conserved in human ESCRT complexes, since the strongest interaction of CHMP6 (the human equivalent of Vps20) was observed with EAP20 (human equivalent of Vps25) in yeast two-hybrid screens (Martin-Serrano et al., 2003; von Schwedler et al., 2003).

ESCRT-II Binds to Lipid Vesicles and Dramatically Increases Binding of Vps20 to Membranes

The work of Emr and colleagues established several important observations concerning cellular localization of ESCRT-II and ESCRT-III complexes. First, the membrane association of ESCRT-II in intact yeast does not depend on ESCRT-III. Second, proper localization of ESCRT-III in yeast does depend on ESCRT-II (Babst et al., 2002b). In light of these observations, we tested binding of ESCRT-II to lipid vesicles in the absence and presence of Vps20. Purified ESCRT-II shows detectable binding to liposomes made of total brain lipids (Figure 5F). Vps20 also shows some binding to the liposomes. However, when mixed together, membrane binding of both ESCRT-II and especially Vps20 dramatically increases (Figure 5F). The same effect, i.e., a dramatic increase in Vps20 binding to liposomes, is observed when Vps20 is mixed with Vps25 (Figure 5G). These

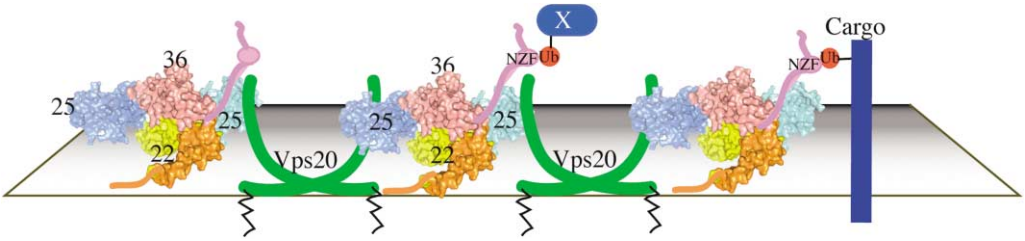

Figure 6. A Model Depicting a Possible Network of Interactions between ESCRT-II and ESCRT-III on the Endosomal Membrane

The Vps36 interaction with either ubiquitinated cargo or another unidentified component of the endosomal machinery would lead to assembly of a cargo/ESCRT-I/ESCRT-II/ESCRT-III complex on the endosomes. The interaction of Vps25 subunit from ESCRT-II with Vps20 on the membrane shown here would serve as a nucleus for assembly of ESCRT-III.

observations are consistent with in vivo data that ESCRT-III membrane localization requires ESCRT-II (Babst et al., 2002a). We do not know which ESCRT-II subunit(s) participates directly in membrane binding. The N-terminal region of Vps22 from various species (equivalent to the first 22 residues preceding the N-terminal helix H1, which are disordered in the crystal structure) is particularly rich in basic residues (~30% in human Vps22) and could be involved in this process. Consistent with this, we observe weak but reproducible binding of the N-terminal helical domain of Vps22 (residues 1–90) to brain-derived liposomes (data not shown), suggesting that Vps22 might contribute to membrane binding of ESCRT-II. Further investigations into lipid specificities and affinities of different ESCRT components are necessary in order to understand spatial and temporal aspects of ESCRT assemblies on membranes.

Conclusions

The structure of the ESCRT-II shows a remarkable, trilobal subunit arrangement, with one lobe containing Vps22/Vps36 sandwiched together side-by-side and each of the other two lobes containing one copy of Vps25. A common building block, the winged helix domain, is repeated eight times in ESCRT-II core structure, giving rise to three lobes of equal length. It is attractive to hypothesize that this could allow for easy build-up of interaction networks on a membrane. We show that ESCRT-II makes direct, strong interactions with Vps20, an ESCRT-III subunit and that this interaction involves the Vps25 subunit. We also show that purified ESCRT-II can bind directly to liposomes in vitro and that this binding very efficiently recruits Vps20 to membranes. Since Vps20 is myristoylated and functions on the membrane (Ashrafi et al., 1998; Babst et al., 2002a), we postulate that the two Vps25 lobes are oriented toward the membrane. For Vps22/Vps36, we have fewer orientation landmarks, but we postulate that the N-terminal segment of Vps22 might contribute to membrane interactions and that this protruding end of the complex serves as a flagstone, rather than a flag. Therefore, all three ESCRT-II lobes may be hovering close to the membrane surface (Figure 6). The ubiquitin binding NZF domain (Alam et al., 2004) in the N-terminal portion of Vps36 (which is not present in the crystal) is connected via a long sequence to the core of ESCRT-II, and it is likely that it would be able to reach either ubiquitinated cargo or an unidentified ubiquitinated component of the sorting machinery in several arrangements of ESCRT-II on the membrane, including the one that we propose. With a structural model in sight, we can start asking specific questions about ESCRT-II function and its links with other components involved in protein sorting and MVB biogenesis.

Experimental Procedures

ESCRT-II Plasmids

The sequences encoding *S. cerevisiae* Vps22, Vps25, and Vps36 were PCR amplified from genomic DNA (ATCC 9763D) and cloned into the coexpression polycistronic vector pOPC, following general cloning strategy described by Tan (2001). The resulting construct has a MetAlaHis$_6$ affinity tag immediately preceding residue Met1 of Vps36, Vps25, or both. Vps22 was cloned into the first cassette, Vps36 into the second cassette, and Vps25 in the third. Ubiquitin and Vps20 were cloned into pOPTG vector to create a fusion protein with an N-terminal GST tag. N-terminal truncations of Vps22 (residues 1–40 deleted) and Vps36 (residues 1–370 deleted) were produced by PCR. N-terminal fragment of Vps22 (residues 1–90) was produced by PCR and cloned into pOPTH to express the protein with an N-terminal His$_6$ tag. All constructs were verified by sequencing.

Protein Expression and Purification

Proteins were expressed in C41(DE3) cells, grown at 37°C to an OD_{600} = 1.0, then induced with 0.3 mM IPTG and incubated at 16°C for 12 hr. Selenomethionine-substituted protein was grown in methionine-requiring B834(DE3) cells in M9 minimal media supplemented with 1 mg/l riboflavin, 1 mg/l niacinamide, 1 mg/l pyridoxine monohydrochloride, 1 mg/l thiamine, 0.4% D (+)-glucose, 2 mM of $MgSO_4$, 25 mg/l of $FeSO_4$, 40 mg/l of each amino acid except methionine, 40 mg/l seleno-L-methionine, and 0.1 g/l ampicillin.

Cells were resuspended in sonication buffer (20 mM Tris [pH 8.0], 50 mM potassium phosphate [pH 8.0], and 100 mM NaCl) and lysed with a French press. After ultracentrifugation, the supernatant was loaded onto Ni^{2+}-affinity column equilibrated with buffer A (20 mM Tris [pH 8.0], 50 mM potassium phosphate [pH 8.0], 100 mM NaCl, 15 mM imidazole, and 0.05% Triton X-100). The column was washed with the same buffer without Triton X-100 and the protein was eluted with an imidazole gradient. Fractions containing ESCRT-II were pooled and diluted with buffer B (20 mM Tris [pH 8.0], 2 mM DTT), loaded onto a Q-Sepharose column, and eluted with a NaCl gradient. Fractions containing ESCRT-II were pooled, concentrated, and purified by gel filtration on Superdex 200 16/60 equilibrated in buffer C (20 mM Tris [pH 7.4], 100 mM NaCl, and 2 mM DTT). The purified ESCRT-II was concentrated to 7 mg/ml for crystallization screens.

The GST-fusion proteins for binding assays were purified on Glutathione Sepharose resin (Amersham). The resin was washed with GST buffer A (50 mM Tris [pH 7.5, 4°C], 1 mM EGTA, 1 mM EDTA, and 2 mM DTT) followed by GST buffer B (50 mM Tris [pH 7.5], 200 mM NaCl, and 2 mM mercaptoethanol). GST-fusion protein was eluted with elution buffer (50 mM Tris [pH 8.5], 10 mM glutathione,

and 2 mM mercaptoethanol). The GST-fusion proteins were concentrated and desalted using PD-10 column from Amersham Biosciences.

Crystallization

Solutions for 1200 crystallization conditions were dispensed into reservoirs of 96-well crystallization plates (Corning, NY). Protein (100 nl) and reservoir (100 nl) solutions were added to the plates as sitting drops using a Cartesian robot (Genomics Solutions, Huntingdon, UK) and incubated at 17°C. Optimal crystals were obtained in 3.1% PEG 35000, 0.1 M Tris acetate (pH 8.5), 1.36 M sodium formate, and 19% glycerol. Crystals used for data collection were grown by adding 10 μl of protein to sitting wells containing 5 μl of silica hydrogel (Hampton Research) preincubated with 5 μl of reservoir solution and 2 μl of additive, either 1 M ammonium sulfate or 0.1 M ATP. Silica hydrogel was made by mixing equal parts of sodium silicate solution (2.8% v/v) with diluted acetic acid. Crystals were cryoprotected by transferring them to cryoprotectant solution containing 3.1% PEG 35000, 0.1 M Tris acetate (pH 8.5), 1.36 M sodium formate, and 22% glycerol before freezing in the cryostream at 100 K.

Data Collection, Phasing, and Model Refinement

Diffraction data were collected at 100 K. A 3.7 Å resolution SAD data set was collected at the peak of the fluorescence spectrum for a dehydrated, selenomethionine-substituted crystal and used for initial phases and model building. Subsequently, a 4 Å resolution Se-Met data set was collected for a crystal that was not dehydrated, and this was used to provide initial phases for a 3.6 Å resolution data set from a native crystal that was not dehydrated. For the Se-Met MAD phasing, data sets were collected at the fluorescence peak, inflection, and remote wavelengths. Intensities were integrated with MOSFLM (Leslie, 1992) and scaled using SCALA (CCP4, 1994). A total of 19 selenium sites (there are 20 non-N-terminal Met residues) were located using the program SnB (Howell et al., 2000; Smith et al., 1998; Weeks and Miller, 1999) and refined with autoSHARP (de La Fortelle and Bricogne, 1997). Solvent flattening was carried out using a solvent content of 71.2% as optimized by SHARP. Table 1 lists statistics for data collection and phase refinement. The phases from the Se-Met MAD data were extended to 3.6 Å using the program DM. The assignment of the sequence to the density was consistent with the Se-Met sites. In addition, a high multiplicity data set was obtained using 2.07 Å wavelength radiation in order to detect sulfur positions by their anomalous scattering (Table 1).

Anomalous difference electron density maps calculated with the long wavelength (2.07 Å) native data set and the Se peak wavelength (0.9793 Å) data set were used to establish unambiguous locations of the Cys and Met residues. The long wavelength anomalous difference map showed sulfur peaks greater than 3σ (average peak height 5σ) for all Cys residues except Vps22 Cys68 and Vps25 Cys181 and for all of the non-N-terminal Met residues. Moreover, each Met residue was associated with a peak greater than 3σ in the Se peak wavelength anomalous difference map (average peak height is 11σ). No Cys residue was associated with a peak in the Se peak wavelength anomalous difference map. The use of these two anomalous difference maps allowed us to identify all of the Cys and Met residues and to differentiate between them. This greatly facilitated building the initial model. Although all three subunits have a similar domain organization, the identities of the polypeptides were unambiguous even from the earliest stages of model building because of the unique patterns of Cys and Met residues in these subunits, which have no sequence conservation. The model was built with the program O (Jones et al., 1991) then optimized with cycles of manual fitting and restrained/TLS refinement with REFMAC (Murshudov et al., 1997). Nine TLS groups were defined corresponding to one group for each of the WH domains and the N-domain of Vps22. The TLS refinement resulted in a lower free R factor than a simple overall B factor refinement. Because of the low resolution, atomic B factors were not refined. Final statistics for all data sets are given in Table 1. There are no residues in the disallowed regions of the Ramachandran plot, and 81% are in the most favored regions as defined by PROCHECK (Laskowski et al., 1993).

The Vps25 WHA domain has the poorest electron density in the complex and was more difficult to interpret. The density in the β1/H3 loop was particularly difficult to interpret. Following strand β1, there is a β-hairpin encompassing residues 50–74 with residues 55–71 not visible. Given that there are no unambiguous experimental sequence markers in this region (no Met and no Cys residues), there is some uncertainty of the sequence register in the 50–79 region of Vps25 WHA. The region from 55 to 74 represents an insertion in the yeast Vps25 relative to other species, so that the 50–74 β-hairpin may be unique to *S. cerevisiae*. There are several regions in which the side chain density is not clear, but the main chain trace is unambiguous. This includes much of the N-domain of Vps22 and the WHB domains from Vps25. In general, the side chain density for larger residues, particularly in the hydrophobic cores and at the intersubunit interfaces, can be discerned.

Pull-Down Assays

For GST pull-downs, glutathione resin in minispin columns (Amersham Biosciences) was prewashed twice with binding buffer (PBS with 0.05% Triton X-100). A 200–250 μg aliquot of GST-tagged protein and 600–700 μg of His-tagged protein were mixed with resin and *E. coli* cytosol (10 mg/ml) in binding buffer. Identical results were obtained when the *E. coli* cytosol was omitted from the assays. The assay mix was incubated for 2 hr at 4°C on a rotating wheel and washed eight times with binding buffer. Bound proteins were eluted with SDS sample buffer and analyzed by SDS-PAGE. For His-tag pull-downs, minispin columns (Perbio) were packed with 40 μl bed volume of talon metal affinity resin (Clontech) equilibrated in binding buffer. Samples were washed with binding buffer containing 20 mM imidazole (pH 8.0), and the bound proteins were eluted with SDS sample buffer.

Liposome Binding Assays

Purified proteins (5 μM) were incubated with 0.5 mg/ml sonicated liposomes in 100 μl reactions. Liposomes were prepared from bovine brain lipid extract (Folch fraction type I, Sigma B1502) in buffer containing 20 mM HEPES (pH 7.4), 150 mM NaCl, and 1 mM DTT. After 15 min incubation at 4°C, reactions were sedimented at 140,000 × g in a Beckman TLA100 rotor for 15 min at 4°C. The supernatants (S) and the pellets (P), resuspended in an equal volume of buffer, were analyzed by SDS-PAGE and Coomassie blue staining. Control proteins, GST, and BSA (Sigma A7638) were used as controls and showed no trace of liposome binding.

Acknowledgments

We thank Joanne McCarthy, Ed Mitchell, Gordon Leonard, Andrew McCarthy, Martin Walsh, Didier Nurizzo, and David Hall for assistance with data collection at ESRF beamlines BM14, ID14-4, ID29, and ID23. We are grateful to J. Helliwell, S. Hasnain, and M. Cianci for beamtime and help on Daresbury SRS NWSGC Station 10 (funded by BBSRC grants 719/B15474 and 719/REI20571 to S. Hasnain and J. Helliwell) and an NWDA project award (N0002170 to M. Cianci). We thank Michael Wilson for stimulating discussions and Brian Peter for liposome preparations. H.T. is supported by the Agency for Science, Technology, and Research of Singapore and B.G. by a fellowship from Secretaría de Estado de Educación y Universidades and cofinanced by the European Social Fund. The work was supported by the MRC (R.L.W.). The PDB ID number for the structure reported in this paper is 1W7P.

Received: August 20, 2004
Revised: September 2, 2004
Accepted: September 7, 2004
Published online: September 16, 2004

References

Alam, S.L., Sun, J., Payne, M., Welch, B.D., Blake, B.K., Davis, D.R., Meyer, H.H., Emr, S.D., and Sundquist, W.I. (2004). Ubiquitin interactions of NZF zinc fingers. EMBO J. *23*, 1411–1421.

Ashrafi, K., Farazi, T.A., and Gordon, J.I. (1998). A role for *Saccharomyces cerevisiae* fatty acid activation protein 4 in regulating protein

N-myristoylation during entry into stationary phase. J. Biol. Chem. *273*, 25864–25874.

Babst, M., Odorizzi, G., Estepa, E.J., and Emr, S.D. (2000). Mammalian tumor susceptibility gene 101 (TSG101) and the yeast homologue, Vps23p, both function in late endosomal trafficking. Traffic *1*, 248–258.

Babst, M., Katzmann, D.J., Estepa-Sabal, E.J., Meerloo, T., and Emr, S.D. (2002a). ESCRT-III: an endosome-associated heterooligomeric protein complex required for MVB sorting. Dev. Cell *3*, 271–282.

Babst, M., Katzmann, D.J., Snyder, W.B., Wendland, B., and Emr, S.D. (2002b). Endosome-associated complex, ESCRT-II, recruits transport machinery for protein sorting at the multivesicular body. Dev. Cell *3*, 283–289.

Bache, K.G., Slagsvold, T., Cabezas, A., Rosendal, K.R., Raiborg, C., and Stenmark, H. (2004). The growth-regulatory protein HCRP1/hVps37A is a subunit of mammalian ESCRT-I and mediates receptor downregulation. Mol. Biol. Cell *15*, 4337–4346.

Bishop, N., and Woodman, P. (2001). TSG101/mammalian VPS23 and mammalian VPS28 interact directly and are recruited to VPS4-induced endosomes. J. Biol. Chem. *276*, 11735–11742.

Bonifacino, J.S., and Traub, L.M. (2003). Signals for sorting of transmembrane proteins to endosomes and lysosomes. Annu. Rev. Biochem. *72*, 395–447.

Bowers, K., Lottridge, J., Helliwell, S.B., Goldthwaite, L.M., Luzio, J.P., and Stevens, T.H. (2004). Protein-protein interactions of ESCRT complexes in the yeast *Saccharomyces cerevisiae*. Traffic *5*, 194–210.

CCP4 (Collaborative Computing Project 4) (1994). The CCP4 suite: programs for protein crystallography. Acta Crystallogr. D *50*, 760–763.

Clark, K.L., Halay, E.D., Lai, E., and Burley, S.K. (1993). Co-crystal structure of the HNF-3/fork head DNA-recognition motif resembles histone H5. Nature *364*, 412–420.

Conibear, E. (2002). An ESCRT into the endosome. Mol. Cell *10*, 215–216.

de La Fortelle, E., and Bricogne, G. (1997). Maximum-likelihood heavy-atom parameter refinement for multiple isomorphous replacement and multiwavelength anomalous diffraction methods. Methods Enzymol. *276*, 472–494.

Dunn, R., and Hicke, L. (2001). Domains of the Rsp5 ubiquitin-protein ligase required for receptor-mediated and fluid-phase endocytosis. Mol. Biol. Cell *12*, 421–435.

Finnin, M.S., Cicero, M.P., Davies, C., Porter, S.J., White, S.W., and Kreuzer, K.N. (1997). The activation domain of the MotA transcription factor from bacteriophage T4. EMBO J. *16*, 1992–2003.

Gajiwala, K.S., and Burley, S.K. (2000). Winged helix proteins. Curr. Opin. Struct. Biol. *10*, 110–116.

Garrus, J.E., von Schwedler, U.K., Pornillos, O.W., Morham, S.G., Zavitz, K.H., Wang, H.E., Wettstein, D.A., Stray, K.M., Cote, M., Rich, R.L., et al. (2001). Tsg101 and the vacuolar protein sorting pathway are essential for HIV-1 budding. Cell *107*, 55–65.

Gruenberg, J., and Stenmark, H. (2004). The biogenesis of multivesicular endosomes. Nat. Rev. Mol. Cell Biol. *5*, 317–323.

Hettema, E.H., Valdez-Taubas, J., and Pelham, H.R. (2004). Bsd2 binds the ubiquitin ligase Rsp5 and mediates the ubiquitination of transmembrane proteins. EMBO J. *23*, 1279–1288.

Hicke, L., and Dunn, R. (2003). Regulation of membrane transport by ubiquitin and ubiquitin-binding proteins. Annu. Rev. Cell Dev. Biol. *19*, 141–172.

Howell, P.L., Blessing, R.H., Smith, G.D., and Weeks, C.M. (2000). Optimizing DREAR and SnB parameters for determining Se-atom substructures. Acta Crystallogr. D *56*, 604–617.

Jones, T.A., Zou, J.-Y., Cowan, S.W., and Kjeldgaard, M. (1991). Improved methods for building protein models in electron density maps and the location of errors in these models. Acta Crystallogr. A *47*, 110–119.

Kamura, T., Burian, D., Khalili, H., Schmidt, S.L., Sato, S., Liu, W.J., Conrad, M.N., Conaway, R.C., Conaway, J.W., and Shilatifard, A. (2001). Cloning and characterization of ELL-associated proteins EAP45 and EAP20. A role for yeast EAP-like proteins in regulation of gene expression by glucose. J. Biol. Chem. *276*, 16528–16533.

Katzmann, D.J., Babst, M., and Emr, S.D. (2001). Ubiquitin-dependent sorting into the multivesicular body pathway requires the function of a conserved endosomal protein sorting complex, ESCRT-I. Cell *106*, 145–155.

Katzmann, D.J., Odorizzi, G., and Emr, S.D. (2002). Receptor downregulation and multivesicular-body sorting. Nat. Rev. Mol. Cell Biol. *3*, 893–905.

Katzmann, D.J., Sarkar, S., Chu, T., Audhya, A., and Emr, S.D. (2004). Multivesicular body sorting: ubiquitin ligase Rsp5 is required for the modification and sorting of carboxypeptidase S. Mol. Biol. Cell *15*, 468–480.

Laskowski, R.A., MacArthur, M.W., Moss, D.S., and Thornton, J.M. (1993). PROCHECK: a program to check the stereochemical quality of protein structures. J. Appl. Crystallogr. *26*, 283–291.

Leslie, A.G.W. (1992). Recent changes to the MOSFLM package for processing film and image plate data. In Joint CCP4 and ESF-EACMB Newsletter on Protein Crystallography (Warrington, UK: Daresbury Laboratory).

Li, L., and Cohen, S.N. (1996). Tsg101: a novel tumor susceptibility gene isolated by controlled homozygous functional knockout of allelic loci in mammalian cells. Cell *85*, 319–329.

Martin-Serrano, J., Yarovoy, A., Perez-Caballero, D., and Bieniasz, P.D. (2003). Divergent retroviral late-budding domains recruit vacuolar protein sorting factors by using alternative adaptor proteins. Proc. Natl. Acad. Sci. USA *100*, 12414–12419.

Morita, E., and Sundquist, W.I. (2004). Retrovirus budding. Annu. Rev. Cell Dev. Biol. *20*, 395–425.

Murshudov, G.N., Vagin, A.A., and Dodson, E.J. (1997). Refinement of macromolecular structures by the maximum-likelihood method. Acta Crystallogr. D *53*, 240–255.

Peschard, P., and Park, M. (2003). Escape from Cbl-mediated downregulation. A recurrent theme for oncogenic deregulation of receptor tyrosine kinases. Cancer Cell *3*, 519–523.

Piper, R.C., and Luzio, J.P. (2001). Late endosomes: sorting and partitioning in multivesicular bodies. Traffic *2*, 612–621.

Pornillos, O., Alam, S.L., Rich, R.L., Myszka, D.G., Davis, D.R., and Sundquist, W.I. (2002). Structure and functional interactions of the Tsg101 UEV domain. EMBO J. *21*, 2397–2406.

Raiborg, C., Rusten, T.E., and Stenmark, H. (2003). Protein sorting into multivesicular endosomes. Curr. Opin. Cell Biol. *15*, 446–455.

Reggiori, F., and Pelham, H.R.B. (2001). Sorting of proteins into multivesicular bodies: ubiquitin-dependent and -independent targeting. EMBO J. *20*, 5176–5186.

Schmidt, A.E., Miller, T., Schmidt, S.L., Shiekhattar, R., and Shilatifard, A. (1999). Cloning and characterization of the EAP30 subunit of the ELL complex that confers derepression of transcription by RNA polymerase II. J. Biol. Chem. *274*, 21981–21985.

Sloper-Mould, K.E., Jemc, J.C., Pickart, C.M., and Hicke, L. (2001). Distinct functional surface regions on ubiquitin. J. Biol. Chem. *276*, 30483–30489.

Smith, G.D., Nagar, B., Rini, J.M., Hauptman, H.A., and Blessing, R.H. (1998). The use of SnB to determine an anomalous scattering substructure. Acta Crystallogr. D *54*, 799–804.

Stuchell, M.D., Garrus, J.E., Muller, B., Stray, K.M., Ghaffarian, S., McKinnon, R., Krausslich, H.G., Morham, S.G., and Sundquist, W.I. (2004). The human endosomal sorting complex required for transport (ESCRT-I) and its role in HIV-1 budding. J. Biol. Chem. *279*, 36059–36071.

Sundquist, W.I., Schubert, H.L., Kelly, B.N., Hill, G.C., Holton, J.M., and Hill, C.P. (2004). Ubiquitin recognition by the human TSG101 protein. Mol. Cell *13*, 783–789.

Tan, S. (2001). A modular polycistronic expression system for overexpressing protein complexes in *Escherichia coli*. Protein Expr. Purif. *21*, 224–234.

Teo, H., Veprintsev, D.B., and Williams, R.L. (2004). Structural insights into endosomal sorting complex required for transport

(ESCRT-I) recognition of ubiquitinated proteins. J. Biol. Chem. *279*, 28689–28696.

Urbanowski, J.L., and Piper, R.C. (2001). Ubiquitin sorts proteins into the intralumenal degradative compartment of the late-endosome/vacuole. Traffic *2*, 622–630.

von Schwedler, U.K., Stuchell, M., Muller, B., Ward, D.M., Chung, H.Y., Morita, E., Wang, H.E., Davis, T., He, G.P., Cimbora, D.M., et al. (2003). The protein network of HIV budding. Cell *114*, 701–713.

Weeks, C.M., and Miller, R. (1999). The design and implementation of SnB v2.0. J. Appl. Crystallogr. *32*, 120–124.